THE JOURNAL OF PHYSICAL CHEMISTRY B

ARTICLE

pubs.acs.org/JPCB

Modeling of Chemical Reactions in Micelle: Water-Mediated Keto−Enol Interconversion As a Case Study

Paolo Marracino,[†] Andrea Amadei,[‡] Francesca Apollonio,[†] Guglielmo d'Inzeo,[†] Micaela Liberti,[†] Antonello di Crescenzo,[§] Antonella Fontana,[§] Romina Zappacosta,[§] and Massimiliano Aschi*[,∥]

[†]Dipartimento di Ingegneria dell'Informazione, Elettronica e Telecomunicazioni, Universita' di Roma 'La Sapienza', Italia

[‡]Dipartimento di Scienze Chimiche, Universita' di Roma 'Tor Vergata', Italia

[§]Dipartimento di Scienze del Farmaco, Università di Chieti "G. d'Annunzio", Italia.

[∥]Dipartimento di Chimica, Ingegneria Chimica e Materiali, Università degli Studi di L'Aquila, Via Vetoio (Coppito 1), 67010 L'Aquila, Italia

Supporting Information

ABSTRACT: The effect of a zwitterionic micelle environment on the efficiency of the keto−enol interconversion of 2-phenylacetylthiophene has been investigated by means of a joint application of experimental and theoretical/computational approaches. Results have revealed a reduction of the reaction rate constant if compared with bulk water essentially because of the different solvation conditions experienced by the reactant species, including water molecules, in the micelle environment. The slight inhibiting effect due to the application of a static electric field has also been theoretically investigated and presented.

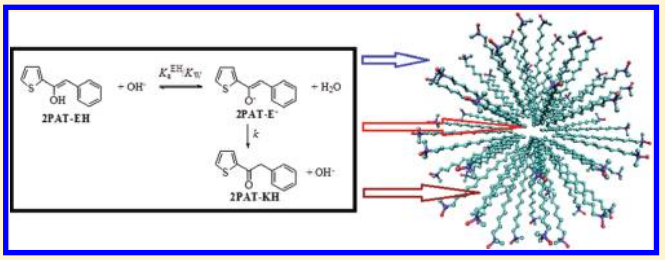

INTRODUCTION

A huge interest in the physics and chemistry of nanoconfined species has emerged in the last years. Both experimental[1−3] and computational studies[4,5] have in fact addressed, for example, the dynamics and thermodynamics effects of the confinement of water molecules in micelles. The interest of these studies relies on the fact that they may not only provide a great help in better understanding the intimate features of biologically relevant interfaces, such as the membranes, but also might open an essentially unexplored scenario of physical and chemical phenomena taking place under somewhat unusual conditions. In particular, the possibility of exploring new chemical pathways deriving from nanoscopic confinement of the reactants has inspired several experimental studies using a wide repertoire of techniques.[6−23] However, much of the chemical information derived in these systems is particularly difficult to be exhaustively understood. One of the major problems in this respect relies in the fact that, differently from the usual dilute solution conditions, a realistic modeling of chemical reactions in micelles using theoretical methods still represents a challenge. The main problem derives from the fact that not only is the structure of the aqueous micelle unknown a priori but also the location of the reactants within the micelle is not predictable. Both of these aspects plausibly affect the chemical event to be studied within the micelle. As a consequence, in such a scenario, a combination of long time-scale classical molecular dynamics (MD) simulations and quantum-mechanical (QM) calculations is strictly mandatory having to solve a problem involving a chemical reaction in a highly complex system.

In the last few years, the study of chemical reactions in complex atomic-molecular environments has been at the center of our attention. In particular, in our laboratory, we have developed a theoretical/computational approach, the perturbed matrix method (PMM),[24,25] which, in conjunction with classical MD simulations, has repeatedly shown to provide a rather reliable tool for addressing chemical reactions[26,27] both in solution[28] and in protein[29,30] environment.

In this Article, we show a joint application of the PMM/MD combination and experimental measurements to study the intramicelle keto−enol interconversion of the enol of 2-phenylacetylthiophene (**2PAT-EH**, Figure 1) to the corresponding keto form (**2PAT-KH**, Figure 1) catalyzed by the presence of a base which provides, as reactant species, the corresponding enolate (**2PAT-E**$^-$, Figure 1).

The same reaction, under dilute aqueous conditions, was recently investigated in our laboratory using the same experimental and PMM/MD computational setup.[31] From such a study, it resulted that the main issue characterizing the reaction efficiency is the formation of an encounter complex between **2PAT-E**$^-$ and two water molecules, followed by an intracluster

Received: February 25, 2011
Revised: April 21, 2011
Published: June 07, 2011

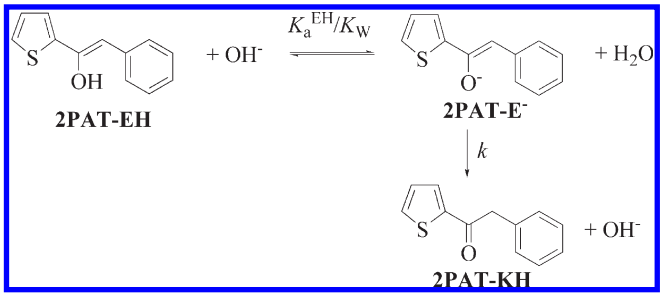

Figure 1. Base-catalyzed keto−enol interconversion of **2PAT**.

mediated proton transfer according to reaction 1

$$\begin{aligned} 2\mathrm{PAT}-\mathrm{E}^{-}_{(aq)} + 2\mathrm{H_2O}_{(l)} &\rightarrow 2\mathrm{PAT}-\mathrm{E}^{-}(\mathrm{H_2O})_{2(aq)} \\ 2\mathrm{PAT}-\mathrm{E}^{-}(\mathrm{H_2O})_{2(aq)} &\rightarrow [\mathrm{TS}(\mathrm{H_2O})_2]_{(aq)} \\ &\rightarrow 2\mathrm{PAT}-\mathrm{EH}-\mathrm{OH}^{-}(\mathrm{H_2O})_{(aq)} \end{aligned} \quad (1)$$

The participation of a different number of water molecules turned out to require very high enthalpic (one water molecule) or entropic (three water molecules) barriers.

In this work, such a reaction scheme is investigated in the presence of an aqueous zwitterionic micelle formed by monomers of an alkyl-*N*,*N*-dimethylamine *N*-oxide(CH_3-$(CH_2)_n$-$NO(CH_3)_2$, **ADAO**), according to reaction 2 both theoretically and experimentally

$$\begin{aligned} 2\mathrm{PAT}-\mathrm{E}^{-}_{(ADAO)} + 2\mathrm{H_2O}_{(ADAO)} &\rightarrow 2\mathrm{PAT}-\mathrm{E}^{-}(\mathrm{H_2O})_{2(ADAO)} \\ 2\mathrm{PAT}-\mathrm{E}^{-}(\mathrm{H_2O})_{2(ADAO)} &\rightarrow [\mathrm{TS}(\mathrm{H_2O})_2]_{(ADAO)} \\ &\rightarrow 2\mathrm{PAT}-\mathrm{EH}-\mathit{OH}^{-}(\mathrm{H_2O})_{(ADAO)} \end{aligned} \quad (2)$$

The choice of using a zwitterionic micelle has mainly been driven by the absence of counterions, which strongly reduces the chemical complexity of the system. More specifically, we have chosen **ADAO** surfactants typically able to form relatively small micelles providing a computationally treatable system. In particular, for the theoretical modeling, we used the *N*,*N*-dimethyl-*N*-tetradecylamine*N*-oxide (**DTAO**, Figure 2), whose aggregation number for spherical micelles has been reported in the literature[32] to be 55. For the experimental measurements, we used the lower homologue *N*-dodecyl-*N*,*N*-dimethylamine *N*-oxide (**DDAO**) with a reported aggregation number of 76.[33]

The slight difference in the simulated and experimentally measured system represented the best compromise for reducing the number of computational or experimental systematic errors. As a matter of fact, **DTAO**, although able to form rather small aggregates, is known to also exhibit a certain tendency to form long cylindrical micelles[34,35] whose presence during the experimental measurements might significantly alter the comparison with the theoretical data where only a spherical micelle has been taken into account. **DDAO** provides a system that is morphologically more easy to control under experimental conditions because it uniquely forms spherical micelles; nevertheless, it presents an aggregation number that is too large for a proper computational treatment. The small difference in the longest alkyl chain of the **DDAO** surfactant should not severely invalidate the comparison between experimental and computational results provided that the overall aggregation structure results in both cases as spherical. Moreover, the difference between the two micelles, relying on their hydrophobicity, is not expected to invalidate severely the present comparison because of the solubilization of the reactant partners in the proximity of the micellar surface[36] (see also infra, Figure 6). Besides, it has been also reported[37] that **ADAO** tends to protonate in acidic media; therefore, we have at hand a reaction (Figure 1) that occurs at basic pH values. It is plausible to disregard protonation considerations of these pH-sensitive surfactants.

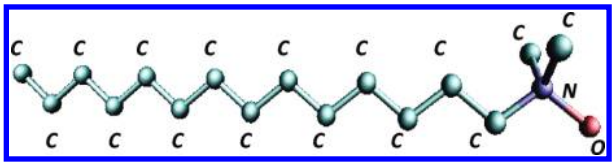

Figure 2. *N*,*N*-Dimethyl-*N*-tetradecylamine-*N*-oxide: zwitterionic micelle monomer used in MD simulations.

After a brief introduction describing the essential features of both experimental setup and theoretical−computational techniques, the results will be presented and commented.

In the last part of the investigation, the preliminary results concerning the effect of a static exogenous electric field on the same route (2) will be briefly outlined. This choice refers to possible practical applications involving a loaded micelle in a general context of drug delivery techniques.

Conventional drug delivery exploits the sensitivity of a nanocarrier to some external stimuli as changes in pH, temperature, and electrolyte concentration to achieve the release of the drug.[38] More recently, attention has been focused on possibilities to assess a controlled release of the drug by an exogenous physical agent, giving rise to an investigation on possible actuators.[39] An intriguing possibility is to use an high exogenous electric field (E-field) to possibly interact with the drug (here roughly modeled with our solute) encapsulated inside the micelle hydrophobic core. For example, in a recent work,[40] the action of an exogenous pulsed E-field acting on an enzymatic reaction taking place in the core of a micelle has been studied, finding a threshold for the applied field, which is able to induce a reversible complete inhibition of the reactive process. The intensities used in ref 40 are comparable to the ones usually adopted in the new emerging technology of pulsed E-fields actually at the base of innovative biomedical applications.[41−47]

EXPERIMENTAL DETAILS

Materials. KCl, *N*-dodecylamine-*N*,*N*-dimethylamine*N*-oxide-(**DDAO**), NaOH, and HCl standard solutions were commercial samples of Analar grade (Aldrich). 2-Phenylacetylthiophene (**2PAT**) was synthesized by the method described in ref 16.

Kinetic Measurements. Rates of ketonization of **2PAT** were measured by partially quenching a freshly prepared solution of the enolate anion (concentration 5×10^{-5} mol dm^{-3}) in 0.5 mol dm^{-3} aqueous NaOH with 0.4 mol dm^{-3}HCl to obtain a final concentration of 0.1 mol dm^{-3}NaOH. The reaction was followed by monitoring the relaxation of the enolate at λ_{max} 343 nm to the more stable keto form. (See Figure 1.) The stopped-flow spectrophotometer was a SFM-400 BioLogic. The measurements were performed in the absence and in the presence of **DDAO** in the range (0.8 to 8.0) $\times 10^{-4}$ mol dm^{-3}.

All kinetic measurements were made at 25.0 ± 0.1 °C and at an ionic strength of 1.0 mol dm^{-3}(KCl).

Ionization Constants. The pK_a^{KH} of **2PAT** was determined spectrophotometrically by monitoring the appearance of the

dx.doi.org/10.1021/jp2018567 |J. Phys. Chem. B 2011, 115, 8102–8111

enolate in solutions of 2.0×10^{-2} mol dm^{-3} **DDAO** with increasing concentration of sodium hydroxide from 0.1 to 1.8 mol dm^{-3}. An apparent pK_b value for each $[OH^-]$ concentration was obtained from absorbance measurements at constant 5×10^{-5} mol dm^{-3} substrate concentration by using eq 3

$$K_b = \frac{(A_{max} - A)[OH^-]}{(A - A_0)} \quad (3)$$

where A, A_o(0.006), and A_{max}(0.812) are absorbances at λ 374 nm at the specified $[OH^-]$ in water and for the fully ionized ketone, respectively. Following previous analogous determinations,[48,49] we have assumed a linear dependence of log K_b on $[OH^-]$ below ca. 2 mol dm^{-3}. A thermodynamic pK_a^{KH} value of 14.09 (±0.02) was obtained by extrapolation to zero $[OH^-]$ of a linear plot of pK_a^{KH}(app) versus $[OH^-]$. (See Table 1.)

Table 1. Determination of the Thermodynamic Value of pK_a^{KH} in the Presence of 2.0×10^{-2} mol dm^{-3} DDAO

[NaOH]/mol dm^{-3}	pK_a^{KH}(app)
0.1	14.11
0.2	14.01
0.4	13.95
0.6	13.95
0.8	13.92
1	13.78
1.2	13.75
1.4	13.71
1.6	13.66
2.0	13.63

COMPUTATIONAL DETAILS

Outline of the Theoretical Strategy. On the basis of the previous study in pure water, we consider reaction 2 to be characterized by two relevant steps:

(i) a preliminary step in which two water molecules and the **2-PAT-E$^-$** species reach a specific geometrical organization (hereafter generally termed as reactive cluster) able to potentially promote an intracluster proton transfer
(ii) the intracluster proton transfer itself

Concerning step i, we assume that, among all two-water-molecules clusters generally indicated as **2PAT-E$^-$(H$_2$O)$_{2(ADAO)}$**, the reactive cluster in the presence of the micelle **(2PAT-E$^-$(H$_2$O)$_2$)*$_{(ADAO)}$** corresponds to a subpopulation geometrically very close to the corresponding gaseous reactive cluster.[31] The rest of the nonreactive clusters **(2PAT-E$^-$(H$_2$O)$_2$)°$_{(ADAO)}$** represents all of the distorted configurations virtually unable to promote the intracluster proton transfer. In light of our previous findings,[31] we also consider these two subpopulations under a pre-equilibrium condition (reaction 4), assuming that the transition kinetics is much faster than step ii.

$$(2PAT\text{-}E^-(H_2O)_2)^\circ_{(ADAO)} \rightleftarrows (2PAT\text{-}E^-(H_2O)_2)^*_{(ADAO)} \quad (4)$$

Within this model, the overall reaction kinetics can be evaluated considering reaction 5

$$(2PAT - (H_2O)_2)^O_{(ADAO)} \overset{K}{\rightleftarrows} (2PAT - E^-(H_2O)_2)^*_{(ADAO)} \xrightarrow{k_{ic}} 2PAT - EH(OH^-)H_2O_{(ADAO)} \quad (5)$$

easily leading to the expression for the overall rate constant in **ADAO**

$$k_{ADAO} = k_{ic}\frac{K}{1+K} \quad (6)$$

in which k_{ic} is the unimolecular rate constant for the intracluster protonation and K is the equilibrium constant for the reaction 4.

The calculation of K can be easily accomplished along MD simulations. (See the Molecular Dynamics Simulations section.) To calculate the k_{ic} rate constant, it is necessary to adopt a QM-based approach to obtain the free-energy barrier for the intracluster proton transfer in the presence of the micelle and of the solvent. This calculation obviously presents many practical difficulties if carried out with a full QM definition of the overall system; therefore, alternative approaches and some approximations are necessary. In this Article, as already stated, the estimation of k_{ic} has been accomplished by using the above-quoted MD-PMM procedure. Details of MD-PMM and related theoretical basis, implications, and assumptions are widely outlined in recent cited literature.[27−29] Nevertheless, for the sake of clarity, we report here both a brief summary of the basic methodological features and a general sequential description of the main steps and approximations used in the present study.

This method, in line with many of the currently employed quantum mechanical/molecular mechanical (QM/MM) strategies is based on the assumption that within a large atomic-molecular system investigated through standard MD simulation, we may define a subportion (termed as quantum centre, QC) whose electronic properties including the reactivity can be obtained by its explicit Born−Oppenheimer electronic states perturbed by the electric field exerted by the rest of the atomic-molecular environment.[24] For this purpose, on the basis of our previous results,[31] we have considered as QC the reactive cluster **(2PAT-E$^-$(H$_2$O)$_2$)*$_{(ADAO)}$** species formed along a classical MD simulation with the presence of the micelle and all of the water molecules acting as an electrostatic (fluctuating) perturbation. The perturbation therefore provides the free energy of intracluster path based on the approximation that the geometries of the species involved along the intracluster reaction path (e.g., reactants, transition state, and products), as obtained under gas-phase conditions, can be considered to be not significantly altered by the presence of the micelle and the aqueous solvent that perturbs the related energies at each MD frame. In this respect, we consider the repertoire of the electrostatic perturbation produced by the micelle and the solvent on the QC along the MD simulation, as statistically significant for all species along the reaction coordinate.[26,27] To summarize, as a consequence of these assumptions,[27] we can obtain the free energy barrier for the intracluster proton transfer by introducing a perturbation of the fluctuating micelle and solvent over the corresponding gas-phase reaction path (by means of PMM) using a single MD simulation ensemble.

The computational steps required for the evaluation of K and k_{ic} are described in the following subsections.

Molecular Dynamics Simulations. We carried out MD simulation of aqueous **ADAO** in the presence of **2PAT-E$^-$** representing the solute. The simulated system consisted of a cubic box in which we placed a single zwitterionic micelle and 14 123 single-point charge (SPC)[50] water molecules, resulting in a typical density of 1000 kg/m^3. The micelle is made of 55 DTAO

dx.doi.org/10.1021/jp2018567 |J. Phys. Chem. B 2011, 115, 8102–8111

monomers (see details in the Supporting Information), experimentally assessed as the critical concentration for micelle formation.[32] The initial structure of the micelle was assumed to be perfectly spherical, as reported in Figure 3. The solute (**2PAT-E**$^-$) was initially put inside the hydrophobic core of the micelle. Following an energy minimization and subsequent solvent relaxation, the system was gradually heated from 50 to 300 K using short (typically 60 ps) MD simulations. A first trajectory was propagated up to 100 ns in a NVT ensemble using an integration step of 2 fs removing the micelle center of mass translation, but with no constraints on its related rotation. The temperature was kept constant at 300 K by the Berendsen thermostat[51] with the same time-step used for the integration algorithm. All bond lengths were constrained using LINCS algorithm.[52] Long-range electrostatics were computed by the particle mesh Ewald method[53] with 34 wave vectors in each dimension and a fourth-order cubic interpolation. The ffG43a1 force field[54] parameters were adopted (details in the Supporting Information). The atomic point charges of solutes and monomers were recalculated by ESP procedure[55] using B3LYP (calculations) and reported in the Supporting Information. For **2PAT-E**$^-$, the same parameters used in ref 31 were adopted. Once we obtained an exhaustive sampling from this trajectory, we selected 15 configurations characterized by having the QC inside the hydrophobic core of the micelle, that is, at distances <1.6 nm from the micelle center of mass. (See below on Figures 5 and 6.) With these initial conditions, we performed 15 parallel simulations (each with a random initial velocity, taken from a Maxwell distribution) with a production time up to 20 ns.

These independent simulations allow us to assess the role exerted by micelle environment on **2PAT** interconversion because solute naturally tends to move from an environment poor of water molecules (the hydrophobic core) toward bulk water.

The principal aim of MD simulations was to provide an estimation of the equilibrium constant (K) for reaction 4. At this purpose, the partial molar free energy variation associated with this reaction ($\Delta\mu_{\text{cluster,ADAO}}$) was calculated using the standard relationship (eq 7)

$$\Delta\mu_{\text{cluster, ADAO}} = -k_B T \ln K = -k_B T \ln \frac{P^*_{2,\text{ADAO}}}{P^{\text{o}}_{2,\text{ADAO}}} \quad (7)$$

where $P^*_{2,\text{ADAO}}$ is the probability of finding the reactive cluster and $P^{\text{O}}_{2,\text{ADAO}}$ is probability of finding the rest of nonreactive clusters along the simulation. The occurrence of the reactive cluster was determined using a cluster-analysis procedure based on the calculation of the root mean square deviation (rmsd) with respect to the optimized gas-phase structure. (See ref 31 and below for further details.) All MD simulations were produced with the Gromacs software.[56]

Perturbed Matrix Method Calculations. As previously described, we extracted from the MD simulation all frames in which we have observed the actual formation of the reactive cluster (**2PAT-E**$^-$**(H$_2$O)$_2$**)$^*_{\text{(ADAO)}}$ species providing the QC for PMM calculation. The QC perturbed electronic ground state was then evaluated by constructing, at each of the previously extracted MD frames, the perturbed electronic Hamiltonian (eq 8)

$$\tilde{H}[\mathbf{r}_n, \mathbf{x}(t)] = \tilde{H}^{\text{o}}(\mathbf{r}_n) + q_T V[\mathbf{r}_{\text{com}}, \mathbf{x}(t)] + \tilde{Z}_1[\mathbf{E}(\mathbf{r}_{\text{com}}, \mathbf{x}(t))] \quad (8)$$

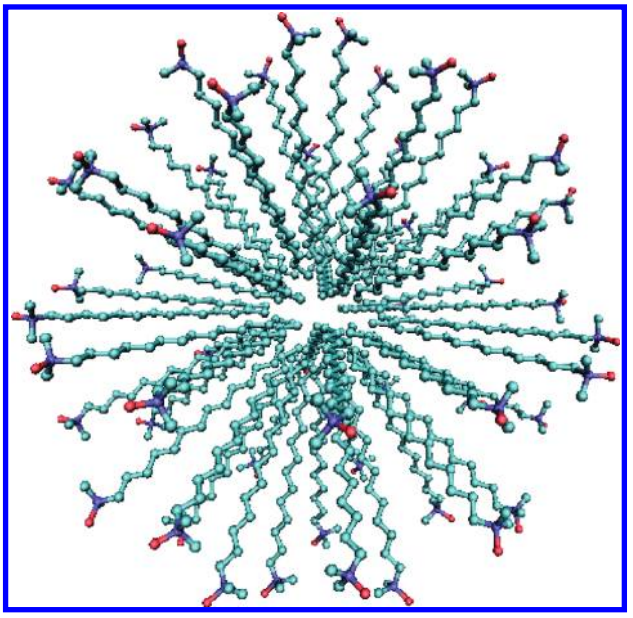

Figure 3. Micelle starting configuration (water molecules not shown).

where $\tilde{H}^{\text{o}}(\mathbf{r}_n)$ is the unperturbed (gas-phase) electronic Hamiltonian calculated for the selected QC geometry (concisely indicated with $\mathbf{r}_n$), q_T is the QC total charge, $V[\mathbf{r}_{\text{com}},\mathbf{x}(t)]$ and $\mathbf{E}$ are the electrostatic potential and electrostatic fields exerted by the micelle and solvent molecules present in the simulation box at their instantaneous $\boldsymbol{x}(t)$ configuration and acting at the QC center of mass ($\mathbf{r}_{\text{com}}$); finally, $\tilde{Z}_1[\mathbf{E}(\mathbf{r}_{\text{com}},\mathbf{x}(t))]$ is a matrix whose generic element is equal to

$$[\tilde{Z}_1]_{l,l'} = -\mathbf{E}\cdot\langle\phi^{\text{o}}_l|\hat{\boldsymbol{\mu}}|\phi^{\text{o}}_{l'}\rangle \quad (9)$$

where $\mathbf{E}$ indicates the perturbing homogeneous electric field exerted by the environment on the QC center of mass, $\hat{\boldsymbol{\mu}}$ is the dipole operator expressed in the unperturbed basis set provided by ϕ^o_l and $\phi^o_{l'}$, that is, the generic unperturbed Hamiltonian matrix eigenvectors corresponding to the lth and l'th unperturbed electronic state, respectively. (See the next subsection.)

Diagonalization of equation 8 at each of the extracted frames allows us to derive the perturbed electronic eigenvalues, $\varepsilon^{(l)}$, representing the perturbed energy of the lth electronic state of the QC in whatever position of the simulation box and interacting with the fluctuating micelle itself and solvent molecules.

Such a procedure is repeated using the unperturbed basis set of different chemical states along the reaction path (i.e., reactants and whatever chemical state X along the reaction path, including TS and products) within the same MD ensemble according to the approximation previously commented. As a result, at each MD frame, we calculated the perturbed ground-state electronic energies for the reactant species (**2PAT-E**$^-$**(H$_2$O)$_2$**)$^*_{\text{(ADAO)}}$ ($\varepsilon^{(0)}{}_{\text{REACTANTS}}$) and for whatever species is along the reaction coordinate ($\varepsilon^{(0)}{}_X$). Such an ensemble of perturbed energies is finally utilized to evaluate the Helmholtz free energy (ΔA), and hence the standard chemical potential ($\Delta\mu$) is the solute density invariant along the reaction coordinate, following standard statistical mechanics relation

$$\Delta\mu_{\text{REACTANTS}\rightarrow X} \cong -k_B T \ln\langle\exp[-\beta(\varepsilon^{(0)}_X - \varepsilon^{(0)}_{\text{REACTANTS}})]\rangle^{\text{O}}_{\text{REACTANTS}} \quad (10)$$

dx.doi.org/10.1021/jp2018567 |J. Phys. Chem. B 2011, 115, 8102–8111

Table 2. Pseudo-First-Order Rate Constants, k_{ADAO}, for the Relaxation of the 2PAT Enolate to the Corresponding Ketone (in the Presence of 0.1 mol dm^{-3}NaOH) and Ionic Strength 1.0 mol dm^{-3} (KCl)

10^{-3} [**ADAO**]/mol dm^{-3}	k_{ADAO}/s^{-1}
0	62.3(±3.7)
0.8	60.0(±6.2)
1.2	50.8(±2.5)
1.6	49.9(±2.6)
2.0	38.3(±1.7)
2.6	35.8(±4.3)
3.0	27.3(±1.5)
4.0	22.4(±1.1)
6.0	14.2(±0.9)
8.0	10.6(±0.6)

where k_B is the Boltzmann constant, the subscript REACTANTS indicates that the average is considered in $(\mathbf{2PAT\text{-}E^-(H_2O)_2})^*_{(ADAO)}$ ensemble (i.e., the ensemble of MD frames in which we have found the reactive cluster formed), and the '0' superscript indicates that we are considering the orthogonal internal vibrational modes as instantaneously relaxed.[27] Note that when X coincides with TS, eq 10 provides the intracluster free energy barrier in the presence of **ADAO** micelle ($\Delta\mu^{\#}_{PMM\text{-}intracluster,ADAO}$) and, in principle, it might be possible to calculate k_{ic}.[31]

The error bar in PMM free-energy calculation was evaluated as standard error dividing the subpopulation of reactive cluster from MD simulation in three portions.

Unperturbed Quantum-Chemical Calculations. The gas-phase (unperturbed) structures of the QC and all other species along the reaction coordinate, including the TS, were first evaluated by applying second-order Moller−Plesset perturbation theory (MP2)[57] in conjunction with the 6-31+G(d) basis set and used to calculate free energies in the gas phase at 300 K using standard statistical mechanics in ideal gas conditions. (See ref 31 for details.) In correspondence of each of these structures, we evaluated the unperturbed electronic states to be used in eq 8 and termed as ϕ_l^o by using time-dependent density functional theory (TD-DFT) calculations[58] using the B3LYP functional and the 6-31+G(d) basis set. We limited our search to the ground-state plus five excited states. (For more details, see the Results section and ref 31.) The Gaussian03[59] and GamessUS[60] packages were used for such calculations.

Calculations with an Exogenous Electric Field. Finally, we also decided to evaluate possible effects induced by high exogenous electric field on the system, hence introducing an uniform E field of 10^6 V/m acting on all atoms in the simulation box, as explained in ref 61. Therefore, all of the above computational procedures were repeated using the MD simulation in the presence of an applied electric field.

RESULTS AND DISCUSSION

For the sake of clarity, because of the slightly different surfactant used for theoretical/computational and experimental studies, the following discussion, when dealing with the surfactant, considers the more general **ADAO** acronym.

Experimental Section. The rate constant of ketonization of the enolate, k_{ADAO}, is sharply depressed by the presence of **ADAO** micelles, as shown in Table 2. It is worth noticing that this effect occurs at **ADAO** concentrations above the critical micelle concentration (cmc = 1.5 × 10^{-3} mol dm^{-3} in pure water),[62] thus highlighting the importance of micelles in order for the effect to be manifested.

Scheme 1. Equilibrium Distribution of the Enolate, 2PAT-E$^-$, between Water and ADAO Micelles

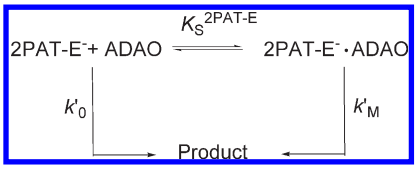

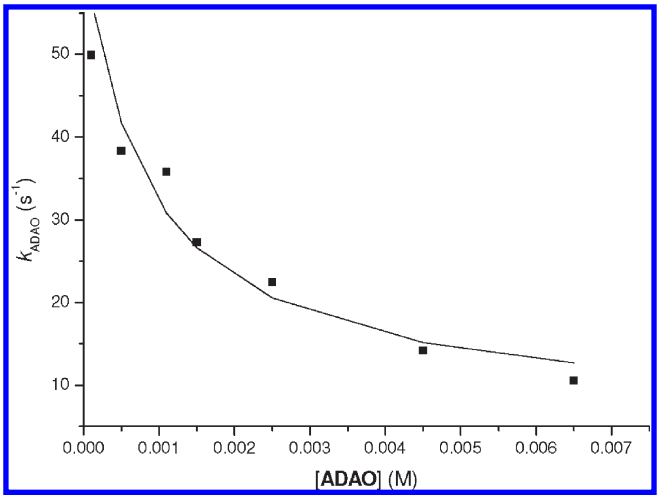

Figure 4. Plot of the experimental first-order rate constants for ketonization of the enolate of **2PAT** in NaOH (0.1 mol dm^{-3}) against the stoichiometric concentration of micellized **ADAO**, fitted into eq 11 (solid line).

Micellar effects upon ketonization reactions under the adopted experimental conditions can be treated[9,63,64] quantitatively in terms of an equilibrium distribution of the enolate, 2PAT-E$^-$, between water and micelles as distinct reaction regions (Scheme 1). In this pseudophase model, $K_S^{2PAT\text{-}E}$ is an association constant with respect to micellized surfactant, **ADAO**, and k'_0 and k'_M are first-order rate constants in aqueous and micellar pseudophases, respectively, which give eq 11.

$$k_{ADAO} = \frac{k'_0 + k'_M K_S^{2PAT-E}[ADAO - cmc]}{1 + K_S^{2PAT-E}[ADAO - cmc]} \qquad (11)$$

A multiple regression analysis of eq 11, by using experimental k_{ADAO}, k'_0, and [**ADAO**] values above cmc and the previously determined cmc value[62] (Figure 4), affords the following results: $K_S^{2PAT\text{-}E}$ = 1160 (±360) dm^3 mol^{-1}, k'_M= 6.2 (±5.0) s^{-1}, and r^2 = 0.92402, highlighting a value of binding constant in perfect agreement with that of 1460(±190) dm^3 mol^{-1} measured[35] for the zwitterionic surfactant 3-(*N*,*N*-dimethyl-*N*-myristylammonium)propanesulfonate.

We could also evaluate a ratio between the two extreme k_{ADAO} values of 0.170 ± 0.014 (details of the standard error calculation are given in the Supporting Information), pointing out a sharp decrease in the ketonization rate in the presence of micelle.

dx.doi.org/10.1021/jp2018567 |*J. Phys. Chem. B* 2011, 115, 8102–8111

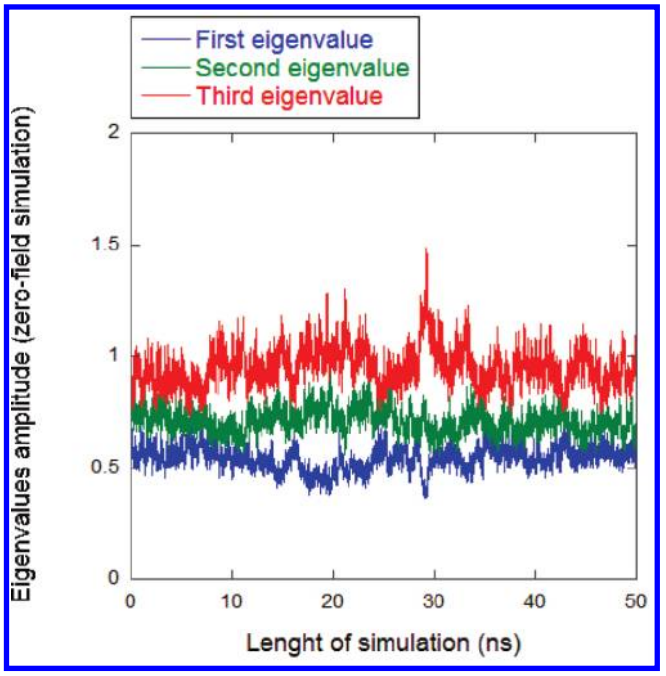

Figure 5. Time course of the three eigenvalues from diagonalization of the covariance matrix.

This observed six-fold decrease may be attributed to a decreased water availability within the micellar aggregate of the neutral **ADAO** surfactant. This is in perfect agreement with the much higher effect (i.e., 40-fold inhibition) measured[16] in the presence of cationic cetyltrimetylammonium bromide (**CTAB**). As a matter of fact, the latter decrease in reactivity was ascribed[16] either to a reduced water availability when micelles are present in the solution or to a strong stabilization of the anionic form of **2PAT-E**$^-$ by cationic **CTAB** micelles, as confirmed by the large decrease in pK_a^{KH} observed in the presence of **CTAB** and the 80-fold lower binding constants, K_S, of the acid with respect to its conjugate base for the cationic surfactant **CTAB**. The lower decrease in pK_a^{KH} of **2PAT** observed in the presence of **ADAO** [pK_a^{KH}(water) − pK_a^{KH}(**ADAO**) = 0.51] with respect to that measured in the presence of **CTAB** micelles [pK_a^{KH}(water) − pK_a^{KH}(CTAB) = 2.25] highlights the minor role of enolate stabilization when dealing with neutral **ADAO** micelles. Nevertheless, both the relatively good fitting of data into eq 11 and the variation of pK_a^{KH} of **2PAT** in the presence of **ADAO** micelles confirm the decisive role of the interaction of the substrate with the micelle, thus allowing us to reject the hypothesis that the observed decrease in the rate of ketonization on passing from water to ADAO micelles was just attributable to an excluded volume effect.

Theoretical. *(a). MD Simulation: Micelle Morphological Analysis and Position of* ***2-PAT-E***$^-$ *within the Micelle.* First of all, we analyze the results from MD simulation of aqueous **ADAO** micelle with the solute **2PAT-E**$^-$. The goal of the first part of this section is to evaluate the shape of the micelle.

To evaluate structural properties of a molecular system, it is often convenient to approximate its geometry to known 3D regions. For this reason, we adopted the covariance matrix method, which provides an immediate path for evaluating dynamical fluctuations of a macromolecular target such as a micelle in a classical 3D space.

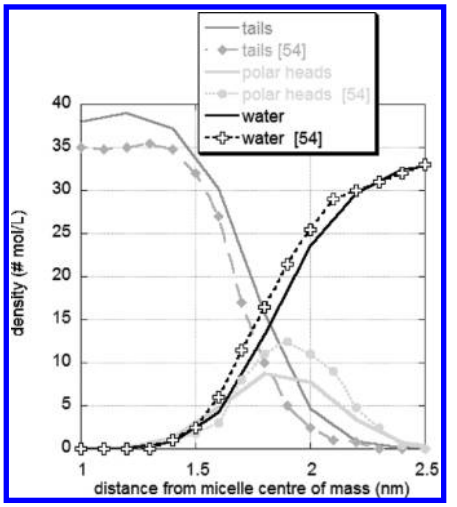

Figure 6. Density profiles of micelle main components from MD simulation.

This method is a direct extension of the most general essential dynamics (ED) analysis, which focuses on seeking those collective degrees of freedom that best approximate the total amount of fluctuation of a dynamical system.[65]

ED is based on a principal component analysis (PCA) of MD-generated structures. The micelle, generally formed by N atoms, can be represented by 3N coordinates. On the basis of our simulation, we construct, at each frame, the 3 × 3 covariance matrix $\tilde{C}$ with diagonal terms defined as, for example, $VAR\,(X) = 1/N\ \Sigma_{i=1}^{N}\ (x_i - \bar{x})^2$ and off diagonal terms defined as, for example, $COV\,(X,Y) = 1/N\ \Sigma_{i=1}^{N}(y_i - \bar{y})(x_1 - \bar{x})$.

Diagonalization of the above matrix provides the corresponding eigenvectors that represent the directions along which the overall system fluctuates with a positional mean square fluctuation given by the corresponding eigenvalues.

The time course of the micelle eigenvalues is reported in Figure 5.

Their relative average magnitude of about 1.3:1.1:1 indicates that the micelle is roughly spherical with individual **ADAO** molecules adopting various nonlinear conformations, predominately in the hydrophilic segment, thereby leading to the overall compact globular shape of the micelle aggregate. These results are consistent with the conventional static picture of a simple spherical micelle with hydrophilic heads out and hydrophobic core inside.

The second goal of this section is to analyze the position of the solute within the micelle.

This does not represent a straightforward task because of the thermally induced morphological fluctuations of the micelle that prevent the identification of a sharp boundary of the system. For this reason, we have based our analysis on the density profile of the main components of the system, that is, water molecules, hydrophilic heads, and hydrophobic tails of the micelle observed along MD simulation. Note that, as previously reported, because of the spherical shape of the micelle, a simple radial density seems to be rather coherent for this purpose. Results reported in Figure 6 indicate that the boundary of the micelle (i.e., the micelle liquid−water interface) can be located between 1.6 and 2 nm from the micelle center of mass. Note that these density profiles are in rather good agreement with the one from Bruce et al.[66] although are obtained with a different micelle.

dx.doi.org/10.1021/jp2018567 |*J. Phys. Chem. B* 2011, 115, 8102–8111

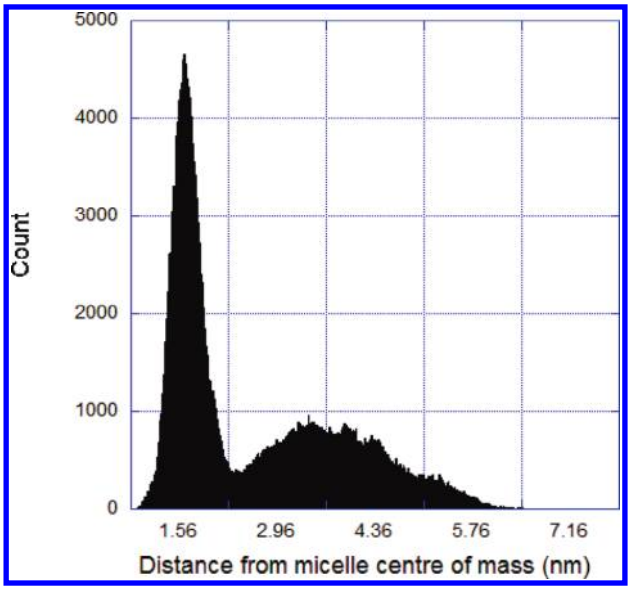

Figure 7. Distribution of the distances between **2-PAT-E**$^-$ and micelle center of mass along MD simulation.

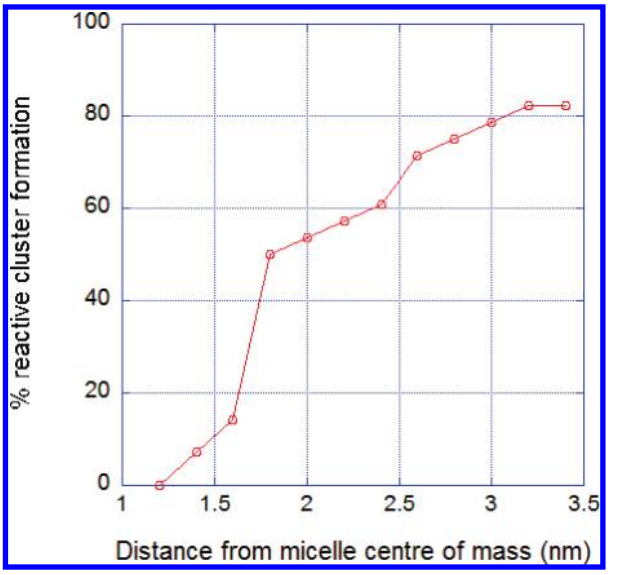

Figure 8. Percentage of reactive clusters formed at different distances from the micelle center of mass with respect to the formation of reactive cluster at whatever position of the box utilized for MD simulation.

We have subsequently analyzed the distance of the solute with respect to the micelle center of mass along the MD simulation. The corresponding distribution, reported in Figure 7, reveals the presence of two regions (two maxima of the distribution). The first one shows a maximum at 1.65 nm with a probability of ~50% of the overall trajectory. A second region, well beyond 2.0 nm, is populated for 50% of the overall trajectory.

On the basis of the results of Figures 6 and 7, we hereafter consider the solute to be inside the micelle when it experiences regions not beyond 1.8 to 1.9 nm from the micelle center of the mass but not much closer than 1.6 nm to the center of mass.

(b). MD Simulation: Formation of 2-PAT-E$^-$*$(H_2O)_2$ Reactive Cluster in the Micelle Interior.* As already reported in the previous sections, the occurrence of the reactive cluster $\mathbf{(2PAT\text{-}E^-\text{-}(H_2O)_n)^*_{(ADAO)}}$ is, within our model, the necessary geometrical condition for the occurrence of the intracluster proton transfer and represents the QC required for PMM calculation. Therefore, we have extracted from the overall MD simulation the frames in which the reactive cluster is formed. As already commented, the procedure followed at this purpose was based on a cluster analysis using the rmsd with respect to the gaseous $\mathbf{(2PAT\text{-}E^-(H_2O)_n)^*}$.[31] In this respect, our previous results,[31] reproducing rather satisfactorily the available experimental data on the reaction kinetics, clearly indicated that the most reliable definition of the reactive $\mathbf{2PAT\text{-}E^-(H_2O)_2}$ cluster population is given by choosing a rmsd threshold equal to 0.06 nm. The probability of formation of these species (expressed in percentage with the overall occurrence in the simulation box) is evaluated at different distances with respect to the micelle center of mass. The result is reported in Figure 8.

From this Figure, we can appreciate a steep transition region, from 1.6 to 2 nm, which, according to the previous results, also roughly indicates the micelle boundaries.

The subpopulation of reactive clusters within the micelle has therefore provided the ensemble to be used for PMM calculations, as reported in the next section.

(c). PMM-MD Calculations on the Intracluster Proton Transfer. On the basis of the gaseous MP2 free energy barrier for the intracluster transition,[31] the PMM free-energy profile of the intracluster reaction in the presence of the micelle were therefore obtained by averaging within the whole ensemble of reactive cluster configurations obtained from MD simulation, as previously explained using eq 10. The obtained free energy barrier, $\Delta\mu^{\#}_{\text{PMM-intracluster,ADAO}}$ schematically compared in Figure 9 with the corresponding quantity obtained in gas-phase and pure water,[31] clearly indicates that the intracluster proton transfer reaction free energy pattern, as obtained in the presence of the micelle, is, within the noise, indistinguishable from the one obtained in bulk water.[31] This finding, depending on the nonrelevant differences between the perturbing electric field exerted by the bulk water and the one exerted by the micelle environment (water and **ADAO** hydrophilic heads) on the QC, suggests that other issues must play a major role in reducing the efficiency of the reaction within the micelle.

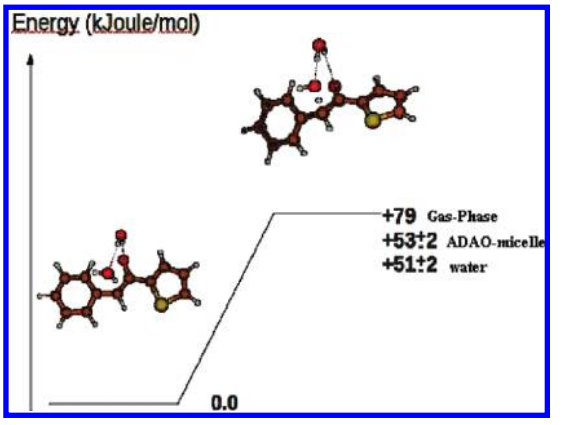

Figure 9. Free-energy diagram of the intracluster reaction in gas-phase,[31] water,[31] and **ADAO** micelle.

In particular, let us consider the adopted reaction model 5 outlined in the methodological section. The present results, similarly to the ones obtained in water, show that the occurrence

of reactive cluster formation requires a relatively high free energy barrier resulting, through eq 7 in a $K \ll 1$. In light of this finding, we can rewrite eq 6 as

$$k_{\mathrm{ADAO}} \approx K k_{\mathrm{ic}} \tag{12}$$

and therefore the overall free energy barrier of the entire process (eq 5) might be approximately considered to be equal to

$$\Delta\mu_{\mathrm{ADAO}} \approx \Delta\mu_{\mathrm{cluster,\,ADAO}} + \Delta\mu_{\mathrm{PMM\text{-}intra\text{-}cluster,\,ADAO}} \tag{13}$$

Moreover, because of the result of Figure 9 from PMM calculations (i.e., $\Delta\mu^{\#}_{\mathrm{PMM\text{-}intracluster,water}} \cong \Delta\mu^{\#}_{\mathrm{PMM\text{-}intracluster,ADAO}}$), it follows that the comparison between the rate constants in **ADAO** micelle and in pure water might be entirely ascribed to the differences in the free energy of formation of the reactive cluster in these environments, that is

$$\begin{aligned}\Delta\Delta\mu &= \Delta\mu_{\mathrm{ADAO}} - \Delta\mu_{\mathrm{water}} \\ &\approx \Delta\mu_{\mathrm{cluster,\,ADAO}} - \Delta\mu_{\mathrm{cluster,\,water}}\end{aligned} \tag{14}$$

that can be calculated using the standard eq 15

$$\Delta\Delta\mu \approx \Delta\mu_{\mathrm{cluster,\,ADAO}} - \Delta\mu_{\mathrm{cluster,\,water}} = -k_{\mathrm{B}}T \ln \frac{P^{*}_{2,\,\mathrm{ADAO}}}{P^{*}_{2,\,\mathrm{water}}} \tag{15}$$

where $P^{*}_{2,\mathrm{ADAO}}$ is the probability of finding the reactive cluster in micelle interior from Figure 8 and $P^{*}_{2,\mathrm{water}}$ is the corresponding probability in water, as found in ref 31. On the basis of such free-energy differences, it is possible to provide an estimation of the overall rate constants ratio between the same reaction in **ADAO** and water using eq 16

$$\frac{k_{\mathrm{ADAO}}}{k_{\mathrm{water}}} \approx \mathrm{e}^{-\Delta\Delta\mu/k_{\mathrm{B}}T} \tag{16}$$

Equation 15 was evaluated as a function of the distance from micelle center of mass as follows: two values of $\Delta\Delta\mu^{\#}$ were evaluated, the first one up to 1.6 nm and the second one up to 1.8 nm (according to the previous approximate definition of micelle interior). Application of eq 14 leads to free-energy values of $\Delta\Delta\mu^{\#}$ (1.6 nm) = 5.9 kJ/mol and $\Delta\Delta\mu^{\#}$ (1.8 nm) = 2.8 kJ/mol, respectively. These values, inserted in eq 15, produce an overall decrease in reaction rate constant between 3.0 and 10.7 times with respect to the reaction in the absence of micelles with a calculated standard error of ±1. (The standard error in PMM calculation was obtained by calculating the standard error using 10 different portions of the total trajectory with a total production time of ~200 ns. See details in the Supporting Information). The theoretical result, reproducing the trend experimentally observed indicates that the effect of the **ADAO** micelle on the reaction efficiency might be entirely ascribed to its inhibiting effect toward water−solute clusterization.

(d). PMM-MD Calculations in the Presence of an Exogenous Electric Field. Finally, we analyzed possible effects induced by E-field on our system, thus performing simulations with an intense (10^6 V/m) E-field.

To justify this intensity, we refer to the previously cited applications of pulsed E-field, which adopts intensities in the range from 10^3 up to 10^6 V/m.

MD simulations gave (data not shown) a statistically significant variation (t test $p < 0.05$) in density profile of water molecules at the inner side of the micelle interface (as previously stated considered between 1.6 and 1.8 nm). The exogenous field seems to overcome the local field produced by nitrogen and oxygen atoms of the polar heads that strictly influence water molecules distribution, thus allowing the micelle to undertake a more ordered configuration with a distribution of hydrophilic head groups located at a greater distance from micelle center of mass with respect to the case of no electric field applied. At the same time, the increase in the core hydrophobicity produces an unfavorable environment for water molecules. PMM calculations also gave an interesting picture of possible inhibitory effect upon reaction efficiency in micelle exerted by the field applied, as already experimentally evidenced.[40]

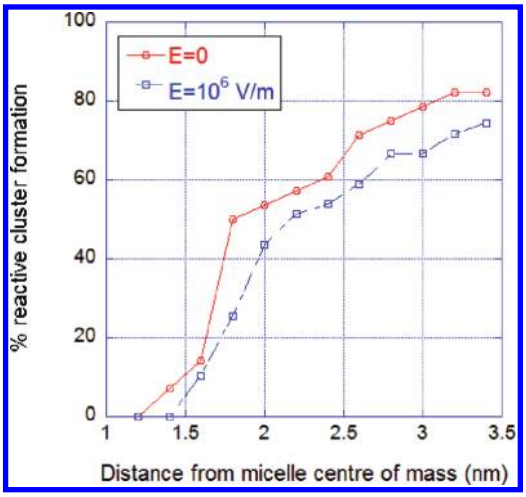

Figure 10. Percentage of reactive clusters at different distances from the micelle center of mass in the presence and in absence of the exogenous electric field.

Figure 10 shows the effect induced by the exogenous E-field on the probability of cluster formation at a given distance from the micelle center of mass, with respect to in-water formation. We can evaluate such effect again using eq 15 obtaining, within the same intervals, $\Delta\Delta\mu^{\#(\mathrm{E\text{-}field})}$(1.6 nm) = 6.3 kJ/mol and $\Delta\Delta\mu^{\#(\mathrm{E\text{-}field})}$(1.8 nm) = 4.0 kJ/mol, which indicates that such an electric field produces an inhibitory effect on the reactive cluster formation. Moreover, by using eq 16, we can estimate that the applied electric field induces a further reaction rate constant decrease due to the combined effect of micelles and applied electric field, reaching a slowing down between 5 and 12.4.

CONCLUSIONS

The effect of a zwitterionic micelle on the efficiency of water-mediated keto−enol interconversion of 2-phenylacetylthiophene has been studied by a joint application of experimental, MD, and perturbed matrix method theoretical−computational techniques. Both experimental and computational results, in good internal agreement, show an inhibiting effect of the micelle with respect to the same reaction in pure water. Analysis of the theoretical results indicates that the proton transfer reaction takes place within an enolate−water cluster in the head-polar region of the micelle, where the reacting partners actually experience environmental conditions, for example, micropolarity effects, very similar to bulk water. As a matter of fact, theoretical results provide a free-energy profile accompanying the intracluster proton transfer reaction virtually identical in pure water and in micelle interior. Consequently, other effects must play an

dx.doi.org/10.1021/jp2018567 |J. Phys. Chem. B 2011, 115, 8102–8111

inhibiting role with respect to the bulk water reaction. Our study has revealed that among other plausible effects the reaction slowing-down might be ascribed to the inhibition of the micelle for the formation of enolate−water cluster, which was demonstrated to be essential for the reaction to occur. This effect is even more amplified in the presence of an electric field whose application is shown to induce a reduction of the density of water in micelle interior, clearly indicating important changes in water partial molar thermodynamics with respect to the bulk conditions.

■ ASSOCIATED CONTENT

Supporting Information. Standard error calculation and TDDNO monomer Gromacs topology. This material is available free of charge via the Internet at http://pubs.acs.org.

■ AUTHOR INFORMATION

Corresponding Author
*E-mail: aschi@caspur.it.

■ ACKNOWLEDGMENT

We wish to thank Caspur Standard HPC grant 2011: Theoretical Study of Electron Transfer Reactions in Complex Atomic-Molecular Systems and MIUR (PRIN2008, prot. 20085M27SS), University "G. d'Annunzio" di Chieti-Pescara. CASPUR (Roma) is acknowledged for the use of Gaussian03. We also wish to acknowledge unknown referees for very helpful comments and advice.

■ REFERENCES

(1) Park, S.; Moilanen, D. E.; Fayer, M. D. *J. Phys. Chem. B* **2008**, *112*, 5279–5290.
(2) Farrer, R. A.; Fourkas, J. T. *Acc. Chem. Res.* **2003**, *36*, 605–612.
(3) Bhattacharyya, K.; Bagchi, B. *J. Phys. Chem. A* **2000**, *104*, 10603–10613.
(4) Faeder, J.; Ladanyi, B. M. *J. Phys. Chem. B* **2001**, *105*, 11148–11158.
(5) Senapati, S.; Berkowitz, M. L. *J. Phys. Chem. A* **2004**, *108*, 9768–9776.
(6) Angulo, G.; Organero, J. A.; Carranza, M. A.; Douhal, A. *J. Phys. Chem. B* **2006**, *110*, 24231–24237.
(7) Heisler, I. A.; Kondo, M.; Meech, S. R. *J. Phys. Chem. B* **2009**, *113*, 1623–1631.
(8) Tielrooij, K. J.; Cox, M. J.; Bakker, H. J. *ChemPhysChem* **2009**, *10*, 245–251.
(9) Bunton, C. A.; Nome, F.; Quina, F. H.; Romsted, L. S. *Acc. Chem. Res.* **1991**, *24*, 357–364.
(10) Romsted, L. S.; Bunton, C. A.; Yao., J. *Curr. Opin. Colloid Interface Sci.* **1997**, *2*, 622–628.
(11) Bianchi, M. T.; Cerichelli, G.; Mancini, G.; Marinelli, F. *Tetrahedron Lett.* **1984**, *25*, 5205–5208.
(12) Mancini, G.; Schiavo, C.; Cerichelli, G. *Langmuir* **1996**, *12*, 3567–3573.
(13) Liou, J.-Y.; Huang, T.-M.; Chang, G.-G. *J. Chem. Soc., Perkin Trans. 2* **1999**, 2171–2176.
(14) Bunton, C. A. *New Compr. Biochem.* **1984**, *6*, 461–504.
(15) Cerichelli, G.; Cerritelli, S.; Chiarini, M.; De Maria, P.; Fontana, A. *Chem.—Eur. J.* **2002**, *8*, 5204–5210.
(16) De Maria, P.; Fontana, A.; Cerichelli, G. *J. Chem. Soc., Perkin Trans. 2* **1997**, 2329–2334.
(17) Schwarze, M.; Milano-Brusco, J. S.; Wille, S.; Mokrushina, L.; Smirnova, I.; Arlt, W.; Schomacker, R. Abstracts of Papers, 239th ACS National Meeting, San Francisco, CA, United States, March 21−25, 2010 (2010), IEC-84.
(18) Xu, B.; Jiang, W.; Li, J.; Zhong, J. *Colloid Polym. Sci.* **2010**, *288*, 347–352.
(19) Ei-Aila, H. J. Y.; Salem, J. K. J. *Tenside, Surfactants, Deterg.* **2003**, *40*, 162–165.
(20) Del Mar Graciani, M.; Rodriguez, A.; Munoz, M.; Moya, M. L. *React. Kinet. Catal. Lett.* **2002**, *76*, 11–18.
(21) Molinero, I.; Sierra, M. L.; Valiente, M.; Rodenas, E. *J. Chem. Soc., Faraday Trans.* **1996**, *92*, 59–63.
(22) Ortica, F.; Elisei, F.; Favaro, G. *J. Chem. Soc., Faraday Trans.* **1995**, *91*, 3405–13.
(23) Taketatsu, T. *Talanta* **1984**, *31*, 805–808.
(24) Aschi, M.; Spezia, R.; Di Nola, A.; Amadei, A. *Chem. Phys. Lett.* **2001**, *344*, 374–380.
(25) Amadei, A.; D'Alessandro, M.; D'Abramo, M.; Aschi, M. *J. Chem. Phys.* **2009**, *130*, 084109.
(26) Amadei, A.; D'Alessandro, M.; Aschi, M. *J. Phys. Chem. B* **2004**, *108*, 16250–16254.
(27) Amadei, A.; Aschi, M.; Di Nola, A. In *Challenges and Advances in Computational Chemistry and Physics*; Canuto, S., Ed.; Springer: 2008; Vol. 6, p 191.
(28) Aschi, M.; D'Abramo, M.; Ramondo, F.; Daidone, I.; D'Alessandro, M.; Di Nola, A.; Amadei, A. *J. Phys. Org. Chem.* **2006**, *19*, 518–530.
(29) Amadei, A.; D'Abramo, M.; Daidone, I.; D'Alessandro, M.; Di Nola, A.; Aschi, M. *Theor. Chem. Acc.* **2007**, *117*, 637–647.
(30) Zazza, C.; Amadei, A.; Palma, A.; Sanna, N.; Tatoli, S.; Aschi, M. *J. Phys. Chem. B* **2008**, *112*, 3184–3192.
(31) Aschi, M.; Zappacosta, R.; De Maria, P.; Siani, G.; Fontana, A.; Amadei, A. *Int. J. Quantum Chem.* **2011**, *111*, 1293–1305.
(32) Gorski, N.; Kalus, J. *J. Phys. Chem. B* **1997**, *101*, 4390–4393.
(33) Herrmann, K. W. *J. Phys. Chem.* **1962**, *66*, 295–300.
(34) Goldsipe, A.; Blankschtein, D. *Langmuir* **2006**, *22*, 9894–9904.
(35) Hoffmann, H.; Oetter, G.; Schwandner, B. *Prog. Colloid Polym. Sci.* **1987**, *73*, 95–106.
(36) De Maria, P.; Fontana, A.; Gasbarri, C.; Siani, G. *Tetrahedron* **2005**, *61*, 7176–7183.
(37) Lair, V.; Bouguerra, S.; Turmine, M.; Letellier, P. *Langmuir* **2004**, *20*, 8490–8495.
(38) Jain, K. K. *Technol. Cancer Res. Treat.* **2005**, *4*, 311–313.
(39) Cohen Stuart, M. A.; S. Huck, W. T.; Genzer, J.; Müller, M.; Ober, C.; Stamm, M.; Sukhorukov, G. B.; Szleifer, I.; Tsukruk, V. V.; Urban, M.; Winnik, F.; Zauscher, S.; Luzinov, I.; Minko, S. *Nat. Mater.* **2010**, *9*, 101–113.
(40) Harada, A.; Kataoka, K. *J. Am. Chem. Soc.* **2003**, *125*, 15306–15307.
(41) Belhradek, M.; Domenge, C.; Luboinski, B.; et al. *Cancer* **1993**, *72*, 3694.
(42) Kubota, Y.; Mir, L. M.; Nakada, T. *J. Urol.* **1998**, *160*, 1426.
(43) Sersa, G.; Cemazar, M.; Rudolf, Z.; Fras, A. P. *Radiol. Oncol.* **1999**, *33*, 291.
(44) Nuccitelli, R.; Pliquett, U.; Chen, X.; Ford, W.; Swanson, J. R.; Beebe, S. J.; Kolb, J. F.; Schoenbach, K. H. *Biochem. Biophys. Res. Commun.* **2006**, *343*, 351–360.
(45) Beebe, S. J.; Fox, P. M.; Rec, L. J.; Somer, K.; Stark, R. H.; Schoenbach, K. H. *IEEE Trans. Plasma Sci.* **2002**, *30*, 286–292.
(46) Zhang, J.; Blackmore, P. F.; Hargrave, B. Y.; Xiao, S.; Beebe, S. J.; Schoenbach, K. H. *Arch. Biochem. Biophys.* **2008**, *471*, 240–248.
(47) Merla, C.; Paffi, A.; Apollonio, F.; Leveque, P.; d'Inzeo, G.; Liberti, M. *IEEE Trans Biomed Eng.* **2011**, *58*, 1294–1302.
(48) Fontana, A.; More O'Ferrall, R. A. *J. Chem. Soc., Perkin Trans. 2* **1994**, 2453–2459.
(49) More O'Ferrall, R. A.; Ridd, J. H. *J. Chem. Soc.* **1963**, 5030–5035.
(50) Berendsen, H. J. C.; Postma, J. P. M.; Gunsteren, W. F. V.; Hermans, J. In *Intermolecular Forces*; Pullman, B., Ed.; Reidel Publishing Company: Dordrecht, The Netherlands, 1981.

(51) Berendsen, H. J. C.; Postma, J. P. M.; van Gunsteren, W. F.; Di Nola, A. *J. Chem. Phys.* **1984**, *81*, 3684–3690.
(52) Hess, B.; Bekker, H.; Berendsen, H. J. C.; Frajie, J. G. E. M. *J. Comput. Chem.* **1997**, *18*, 1463–1472.
(53) Darden, T. A.; York, D. M.; Pedersen, L. G. *J. Chem. Phys.* **1993**, *98*, 10089.
(54) Van Gunsteren, W. F.; Billeter, S. R.; Eising, A. A.; Hunemberger, P. H.; Kruger, P.; Mark, A. E.; Scott, V. R. P.; Tironi, I. G. *Biomolecular Simulation: The GROMOS96 Manual and User Guide*; Hochschlverlag AG an der ETH: Zurich, Switzerland,1996.
(55) Breneman, C. M.; Wiberg, K. B. *J. Comput. Chem.* **1990**, *11*, 361–373.
(56) Van der Spoel, D.; van Buren, A. R.; Apol, E.; Meulenhoff, P. J.; Tieleman, D. P.; Sijbers, A. L. T. M.; van Drunen, R.; Berendsen, H. J. C. *Gromacs User Manual*, version 1.3; Groningen, 1996.
(57) Moller, C.; Plesset, M. S. *Phys. Rev.* **1934**, *46*, 618–622.
(58) Marques, M. A. L.; Gross, E. K. U. *Annu. Rev. Phys. Chem.* **2004**, *55*, 427–455.
(59) Frisch, M. J.; Trucks, G. W.; Schlegel, H. B.; Scuseria, G. E.;Robb, M. A.; Cheeseman, J. R.; Montgomery, J. A., Jr.; Vreven, T., Kudin, K. N.; Burant, J. C.; Millam, J. M.; Iyengar,S. S.; Tomasi, J.; Barone, V.; Mennucci, B.; Cossi, M.;Scalmani, G.; Rega, N.; Petersson, G. A.; Nakatsuji, H.;Hada, M.; Ehara, M.; Toyota, K.; Fukuda, R.; Hasegawa, J.;Ishida, M.; Nakajima, T.; Honda, Y.; Kitao, O.; Nakai, H.;Klene, M.; Li, X.; Knox, J. E.; Hratchian, H. P.; Cross, J. B.;Adamo, C.; Jaramillo, J.; Gomperts, R.; Stratmann, R. E.;Yazyev, O.; Austin, A. J.; Cammi, R.; Pomelli, C.; Ochterski,J. W.; Ayala, P. Y.; Morokuma, K.; Voth, G. A.; Salvador,P.; Dannenberg, J. J.; Zakrzewski, V. G.; Dapprich, S.; Daniels,A. D.; Strain, M. C.; Farkas, O.; Malick, D. K.; Rabuck,A. D.; Raghavachari, K.; Foresman, J. B.; Ortiz, J. V.; Cui,Q.; Baboul, A. G.; Clifford, S.; Cioslowski, J.; Stefanov, B. B.; Liu, G.; Liashenko, A.; Piskorz, P.; Komaromi, I.; Martin,R. L.; Fox, D. J.; Keith, T.; Al-Laham, M. A.; Peng, C. Y.; Nanayakkara, A.; Challacombe, M.; Gill, P. M. W.; Johnson,B.; Chen, W.; Wong, M. W.; Gonzalez, C.; Pople, J. A. *Gaussian 03*, revision C.02; Gaussian, Inc.: Wallingford, CT, 2004.
(60) Schmidt, M. W.; Baldridge, K. K.; Gordon, M. S.; Jensen, J. H.; Koseki, S.; Matsunaga, N.; Nguyen, K. A.; Su, S.; Windus, T. L.; Dupuis, M.; Montgomery, J. A. *J. Comput. Chem.* **1993**, *14*, 1347–1363.
(61) Apollonio, F.; Liberti, M.; Amadei, A.; Aschi, M.; Pellegrino, M.; D'Alessandro, M.; D'Abramo, M.; Di Nola, A.; d'Inzeo, G. *IEEE Trans. Microwave Theory Tech.* **2008**, *56*, 11.
(62) Imaishi, Y.; Kakehashi, R.; Nezu, T.; Maeda, H. *J. Colloid Interface Sci.* **1998**, *197*, 309–316.
(63) Romsted, L. S. In *Surfactants in Solution*; Mittal, K. L., Lindman, B., Eds.; Plenum Press: New York: 1984; Vol. 2, p 1015.
(64) Bunton, C. A.; Savelli, G. *Adv. Phys. Org. Chem.* **1986**, *22*, 213–309.
(65) Amadei, A.; Linssen, A. B. M.; Berendsen, H. J. C. *Proteins: Struct., Funct., Genet.* **1993**, *17*, 412–425.
(66) Bruce, C. D.; Senapati, S.; Berkowitz, M. L.; Perera, L.; Forbes, M. D. E. *J. Phys. Chem. B* **2002**, *106*, 10902–10907.